



Cooling chip on PCB by embedded active microchannel heat sink

Yun-Hao Peng^b, Dai-Hua Wang^{a,b,*}, Xin-Yu Li^b, Ying Zhang^b



^a Key Laboratory of Optoelectronic Technology and Systems of the Ministry of Education of China, Chongqing University, Chongqing 400044, China
^b Precision and Intelligence Laboratory, Department of Measurement and Control Technology and Instrument, Chongqing University, Chongqing 400044, China

ARTICLE INFO

Article history:

Received 8 April 2022

Revised 18 June 2022

Accepted 14 July 2022

Available online 22 July 2022

Keywords:

Thermal management of chip

Cooling chip

Piezoelectric micropump

Microchannel heat sink

Printed circuit board process

ABSTRACT

The use of chips is inseparable from printed circuit board (PCB), therefore, it is an effective way to realize microchannel heat sink (MCHS) on PCB to actively cool chip. For improving the integration and cooling efficiency, and reducing the size, energy consumption and coolant consumption of cooling system for thermal management of chips on PCB, the principle and structure of cooling chip on PCB by embedded active microchannel heat sink (EAMCHS) are proposed. EAMCHS is formed by simultaneously integrating MCHS, diffuser/nozzle piezoelectric micropump (PMP) and piezoelectric microvalves with annular boundary on PCB. Chip to be cooled is mounted directly on MCHS. PMP and piezoelectric microvalves enable EAMCHS to drive and control coolant, respectively. The finite element simulation model and theoretical model of cooling chip on PCB by EAMCHS are established to simulate and analyze its heat transfer characteristics and flow characteristics. The manufacturing and assembly based on PCB process are studied and EAMCHS is manufactured. The size and weight of the assembled EAMCHS are small (about 6.5 cm³) and light (about 18.2 g), respectively. Utilizing high temperature co-fired ceramic (HTCC) to simulate chip heating, the working performances of cooling chip on PCB by EAMCHS are experimentally tested and analyzed on the constructed experimental setup. Research results show that EAMCHS can control the temperature of HTCC at 64.0 °C with heat flux of 50 W/cm² through the flow rate of 30.11 mL/min of coolant. The established theoretical model can describe heat transfer characteristics and flow characteristics of cooling chip by EAMCHS, which will be conducive to its structural design and optimization. The proposed EAMCHS has low energy consumption, small size and light weight, and provides a novel principle, novel method and novel structure for thermal management of chips highly integrated on PCB.

© 2022 Elsevier Ltd. All rights reserved.

1. Introduction

With the rapid development of microelectronic technology and telecommunication, chips toward to high operation speed, high working frequency and small size, causing heat flux of chips have been increasing when they work and bring a new challenge to thermal management of chips [1]. When chips work, if their internal heat cannot be effectively taken away, their performance and reliability will be affected. In severe cases, chips will produce local hot spots to burn them. Therefore, it is necessary to research the principle and method of efficient thermal management of chips to meet the increasing heat dissipation demand of them.

Tuckerman and Pease [2] used microchannel heat sink (MCHS) to research heat transfer from very-large-scale integration (VLSI) in 1981. Since then, more and more researchers have begun to research heat transfer of MCHS [3–5]. The core research of ther-

mal management of chips based on MCHS is how to maximize heat transfer of chips under the premise of smaller flow rate of coolants and energy consumption of cooling systems [6,7]. Accordingly, researches on thermal management of chips based on MCHSs can be divided into three areas as follows: 1) researching the structure of MCHSs with optimal heat transfer performance [8–10], 2) researching coolant with greater specific heat capacity, such as using nanofluid with higher heat transfer efficiency as coolant [11–14] and 3) researching flow boiling of coolant so that it can take away more heat [15,16]. In researches on structure of MCHSs, Collins et al. [17] proposed a novel structure of permeable membrane MCHS based on AlSi10Mg, which can provide lower thermal resistance and pressure drop compared to the manifold MCHS. Tan et al. [18] proposed a MCHS with spider netted structure based on 6063 aluminum to make the maximum temperature difference of high temperature co-fired ceramic (HTCC) reach 9.9 °C when the flow rate of coolant is 0.1 L/min and the heat flux of HTCC is 100 W/cm². Zhai et al. [19] designed a novel double-layered MCHS to reduce its pressure drop and maintain good heat transfer performance. Wang et al. [20] proposed three pin fin MCHSs for cooling

* Corresponding author.

E-mail address: dhwang@cqu.edu.cn (D.-H. Wang).

CPU with centered vertical jet inlets and multiple outlets, and the effects of inlets and outlets position on heat transfer performance of these MCHSs were researched. Katz et al. [21] manufactured a multi-layered printed-circuit heat exchanger (PCHE) with zig-zag flow pattern by vacuum process engineering using dual-certified 316/316 L stainless steel plate stock, and measured heat transfer and pressure drop of PCHE were provided by using supercritical CO₂ and helium. In researches on nanofluid in MCHS, Sarafraz et al. [22] researched the effect of mass concentrations of silver-water nanofluid on thermal performance of rectangular MCHS based on copper. The results show that the overall thermal performance of cooling system is the optimum when the Reynolds number is 1400 and the mass concentration of silver-water nanofluid is 0.05. Arani et al. [23] researched laminar flow and heat transfer of nanofluid water/single-wall carbon nanotube in double-layered MCHS. The results show that with increasing of nanoparticle volume fraction and decreasing of dimensionless values of truncated length, all the thermal resistance of microchannel bottom wall, the ratio of the maximum and the minimum temperature difference of microchannel bottom wall and the ratio of thermal resistance will decrease. Ali and Arshad [24] researched the heat dissipation of water based graphene nanoplatelets nanofluid in MCHSs with different channel angles. The results show that the MCHS with channel angle of 22.5° had the lowest convective thermal resistance. Naranjani et al. [25] employed MCHS with corrugated channels and water-Al₂O₃ nanofluids to make the surface temperature of the heat sink lower and limit thermally induced deformations. The results show that the heat dissipation performance of the proposed MCHS was 22% to 40% higher than that of the water-cooled MCHS with straight channels. In researches on flow boiling of coolant, Radwan et al. [16] designed the optimal headers of a monolithic double-layer MCHS operating under forced convective boiling conditions to make MCHS realize uniform cooling for chips. The results show that the proposed MCHS with the header can make chip have low and uniform temperature. Oudah et al. [26] researched the effects of various configurations of inlet restrictors on the thermal hydraulic performance of flow boiling in MCHS. The results show that the optimum design of MCHS mainly depended on the operational parameters. Mathew et al. [27] researched a novel MCHS, so that coolant can realize the stable flow boiling and improve the cooling performance of MCHS.

In the current researches on cooling systems based on MCHSs for thermal management of chip, almost all of cooling systems drive coolant to flow in MCHSs by utilizing external pumps. Sarafraz and Arjomandi [28] chose a customized peristaltic pump (purchased from Parker) to provide driving force for nano-suspension of copper oxide-indium with thermal performance index of 1.43 in MCHS. Babar and Ali [29] used an alternating current pump (type: VSS 950, Pakistan) to provide the driving force for nanofluid of iron oxide (Fe₂O₃) and titania (TiO₂) in MCHS. In the experiment, they found that compared with distilled water, when the heating power is 55 W, the maximum enhancement of pumping powers with the nanofluids of TiO₂ and Fe₂O₃ were 30.5% and 42.46%, respectively. Deng et al. [30] used a magnetically coupled gear pump (type: GA-T23-DB-380B, Micro-pump) to research the flow boiling heat transfer of deionized water and ethanol in pin fin-interconnected reentrant microchannel (PFIRM). The research results will contribute to boil heat transfer enhancement of PFIRM. Abo-Zahhad et al. [31] used two dual-syringe pumps (type: KDS210, Scientific, Inc.) to research flow boiling heat transfer of ethanol, acetone and Novec-7000 coolants in MCHS. In the experiment, they found that the boiling point was a critical parameter in the system performance of flow boiling-cooling. Xu et al. [32] used an external peristaltic pump to provide driving force for graphene oxide particles nanofluid in a novel MCHS, and the relationship between pump power and heating power was summarized. Mean-

Nomenclature

A	cross-sectional area of MCHS
a	width of MCHS
b	height of MCHS
c	wall width of MCHS
c_p	specific heat of coolant
d_h	hydraulic diameter of MCHS
h	heat transfer coefficient
l	length of inlet (or outlet) of PMP
l_c	length of MCHS
l_F	length of FCSCF
l_i	width of inlet of PMP
l_l	length of IAGCF
l_o	width of PMP outlet
q_{p-c}	flow rate of PMP
r_a	radius of annular boundary
r_p	radius of pump chamber
r_{i-o}	radius of inlet (or outlet)
r_v	radius of valve chamber
t_{in}	temperature of MCHS inlet
t_{chip}	temperature of chip
Re	Reynolds number
Nu	Nusselt coefficient
Pr_{in}	Prandtl Number

Greek symbols

α	surface area multiplication factor
η	efficiency of MCHS
α_1	angle of IAGCF
ρ_l	coolant density
μ_{in}	coolant dynamic viscosity
λ_{in}	thermal conductivity of coolant
λ_w	thermal conductivity of MCHS

Subscript

a	annular boundary
c	channel
i	in
l	liquid
o	out
p	piezoelectric micropump
v	valve
$p-c$	piezoelectric micropump to channel

Acronyms

CPUA	circular piezoelectric unimorph actuator
EAMCHS	embedded active microchannel heat sink
FCSCF	fluid channel of stable coolant flow
HTCC	high temperature co-fired ceramic
MCHS	microchannel heat sink
IAGCF	inclination angle of guided coolant flow printed circuit board
PCB	printed circuit board
PMP	piezoelectric micropump

while, most of external pumps used in the researches are commercially available pumps. Although commercially available pumps have advantage of high reliability, they also have the disadvantages of fixed structure, large size and unable to change the structure according to actual heat dissipation of chips, resulting in the large size of cooling system based on MCHS for thermal management of chip. Moreover, these pumps and MCHSs in cooling systems have to be usually connected by a long pipeline, so that each component of cooling system are relatively dispersed, the integration of

cooling system is low. Accordingly, cooling system needs a lot of energy to overcome the frictional head loss when coolant flows in the pipeline, resulting in high overall energy consumption of it.

As mentioned above, a lot of meaningful researches on thermal management of chip from structures, coolants, principles and methods of heat transfer have been done, but **there are few researches on the principle and system of integrated thermal management of chip.** Meanwhile, almost all of chips are finally installed on printed circuit board (PCB). **However, most of researches on thermal management of chip based on MCHS are not well compatible with chip, whether from material, structure or manufacturing process of MCHS, resulting in most of the current researches cannot actually guide thermal management of chip.** Therefore, it is necessary to find novel principles, novel methods and novel structures for thermal management of chip based on MCHS with structure and manufacturing process compatible with chip to realize chip heat dissipation with higher integration, higher cooling efficiency, lower energy consumption and fewer coolant consumption of cooling system. The use of chips is inseparable from PCB, therefore, it is an effective way to realize MCHS on PCB to actively cool chip.

To solve the above problems, the principle and structure of cooling chip on PCB by **embedded active microchannel heat sink (EAMCHS)** are proposed. The structural principle of EAMCHS are researched, and the EAMCHS with fluid coupling mode of fluid channel of stable coolant flow (FCSCF) and inclination angle of guided coolant flow (IAGCF) in series is designed. By establishing the finite element simulation model and theoretical model of cooling chip on PCB by EAMCHS, the working performances of EAMCHS are simulated and analyzed based on finite element method (FEM) and numerical method. Meanwhile, an experimental setup is established to test cooling chip on PCB by EAMCHS, and the experimental results are compared and analyzed with results of finite element simulation and numerical simulation.

2. Principle

2.1. Principle of cooling chip on PCB by EAMCHS

Fig. 1 shows schematic diagrams of the principle and structure of cooling chip on PCB by EAMCHS. Fig. 1(a) to 1(c) show the schematic diagrams of three-dimensional (3D) integration principle, two-dimensional (2D) structural principle and 3D exploded drawing, respectively. Fig. 1(d) to 1(f) show the structural diagram of PCB substrate of EAMCHS, sectional view of PMP of EAMCHS and the 3D exploded drawing of MCHS with chip to be cooled, respectively. From Fig. 1(a) to 1(c), **EAMCHS is mainly composed of MCHS and PMP in series, chip to be cooled is mounted directly on MCHS to realize the heat transfer with coolant inside MCHS, and the heat is taken away by letting coolant flow rapidly to realize active cooling.** Therefore, the coolant input of MCHS is that output of PMP, and **the fluid coupling between PMP and MCHS is achieved by connecting FCSCF and IAGCF in series.** Moreover, piezoelectric microvalves are arranged at the inlet of PMP and outlet of MCHS, respectively. **In this way, EAMCHS sucks the coolant from inlet valve through PMP, then couples the coolant into MCHS through FCSCF and IAGCF to achieve a rapidly and fully uniform flow, and finally discharges the coolant from the outlet valve.** Through MCHS, the coolant realizes the rapid heat transfer with chip to achieve chip cooling. Meanwhile, **EAMCHS can realize the active control of the coolant by changing amplitude and frequency of the driving voltage applied to PMP and piezoelectric microvalves, and accordingly realize the active control of its heat dissipation performance and the active cooling of chips.** Based on this, EAMCHS can be divided into three modules as follows: 1) the chip cooling module with the MCHS as the core, 2) the fluid driving module with PMP as the

core and 3) the fluid coupling module with FCSCF and IAGCF as the core to connect chip cooling module and fluid driving module. To ensure that the coolant can flow in the MCHS, the differential pressure p_4 minus p_5 between its inlet and outlet is required to be greater than zero, where p_4 and p_5 represent the pressure at the inlet of MCHS (or PMP outlet) and the outlet of MCHS, respectively. To ensure that PMP can pump out coolant, the differential pressure p_2 minus p_4 between its inlet and outlet is required to be greater than zero, where p_2 is the pressure at the inlet of PMP.

From Fig. 1(b), 1(c) and 1(d), **the MCHS of EAMCHS is directly manufactured on PCB by PCB process.** From Fig. 1(d), the MCHS designed as rectangular structure, which is directly covered by chip that need heat dissipation. That is to say, the bottom of cooled chip is also acted as the cover of the MCHS to some extent. The function of the MCHS is to realize the rapid heat transfer between the coolant and the chip, and the heat generated by chip during operation is taken away efficiently by letting the coolant flow rapidly inside it.

From Fig. 1(c) and 1(d), the diffuser/nozzle PMP in the fluid driving module of EAMCHS is composed of **a pump chamber on PCB, polydimethylsiloxane (PDMS) and circular piezoelectric unimorph actuator (CPUA)** to make EAMCHS have high output flow rate. **Piezoelectric microvalve is active control piezoelectric microvalves with annular boundary [33],** which is composed of a valve chamber on PCB, PDMS and CPUA. Though the piezoelectric microvalves, EAMCHS can improve the control accuracy of the coolant flow rate, and can realize the purpose of high precision thermal management of chips. Under the action of driving voltage, CPUA can arch upward and downward alternately by inverse piezoelectric effect to change the volume of the pump chamber, thus the pressure inside the pump chamber is changed to drive the flow of the coolant in EAMCHS. According to the principle of diffuser/nozzle PMP [34,35], when CPUA arches upward, the differential pressure Δp_d ($= p_2 - p_3$) produced by PMP at its inlet is greater than zero and is the differential pressure of the diffuser. This differential pressure allows the coolant to enter the pump chamber from the outside through inlet of EAMCHS. Meanwhile, in this case, the differential pressure Δp_n ($= p_4 - p_3$) produced by PMP at its outlet is greater than zero and is the differential pressure of the nozzle. **This differential pressure allows the coolant into the pump chamber from MCHS.** When CPUA arches downward, the differential pressure Δp_d ($= p_3 - p_4$) produced by PMP at its outlet is greater than zero, and allows the coolant into MCHS from the pump chamber to dissipate the heat of chip. Meanwhile, in order to ensure that the coolant can flow fully uniformly in MCHS to cool the chip uniformly, FCSCF and IAGCF in series are designed to couple PMP and MCHS. A polymethyl methacrylate (PMMA) sheet mounted on the top front side of the EAMCHS not only acts as a cover plate of MCHS, FCSCF, IAGCF and diffuser/nozzle of PMP to form a closed and continuous coolant channel with the bottom of cooled chip, but also presses CPUA on the pump chamber and cooled chip on the MCHS to the copper foil of PCB.

From Fig. 1, in EAMCHS, the outlet of PMP is connected with the inlet of MCHS to form an integrated structure, which can improve the integration and reduce the size of the cooling system. Moreover, the long pipeline connecting pump with MCHS is removed, which can allow the coolant to enter MCHS from pump with the shortest flow path, so that the frictional head loss and the energy consumption of cooling system can be minimized.

Table 1 lists the geometrical parameters of EAMCHS, which is designed according to the structural principle shown in Fig. 1. Among them, to optimize the working performance of EAMCHS, the MCHS is designed and optimized according to [2] and PCB processing standards, the inlet of the MCHS is designed and optimized according to [16]. The diffuser/nozzle PMP is designed and opti-

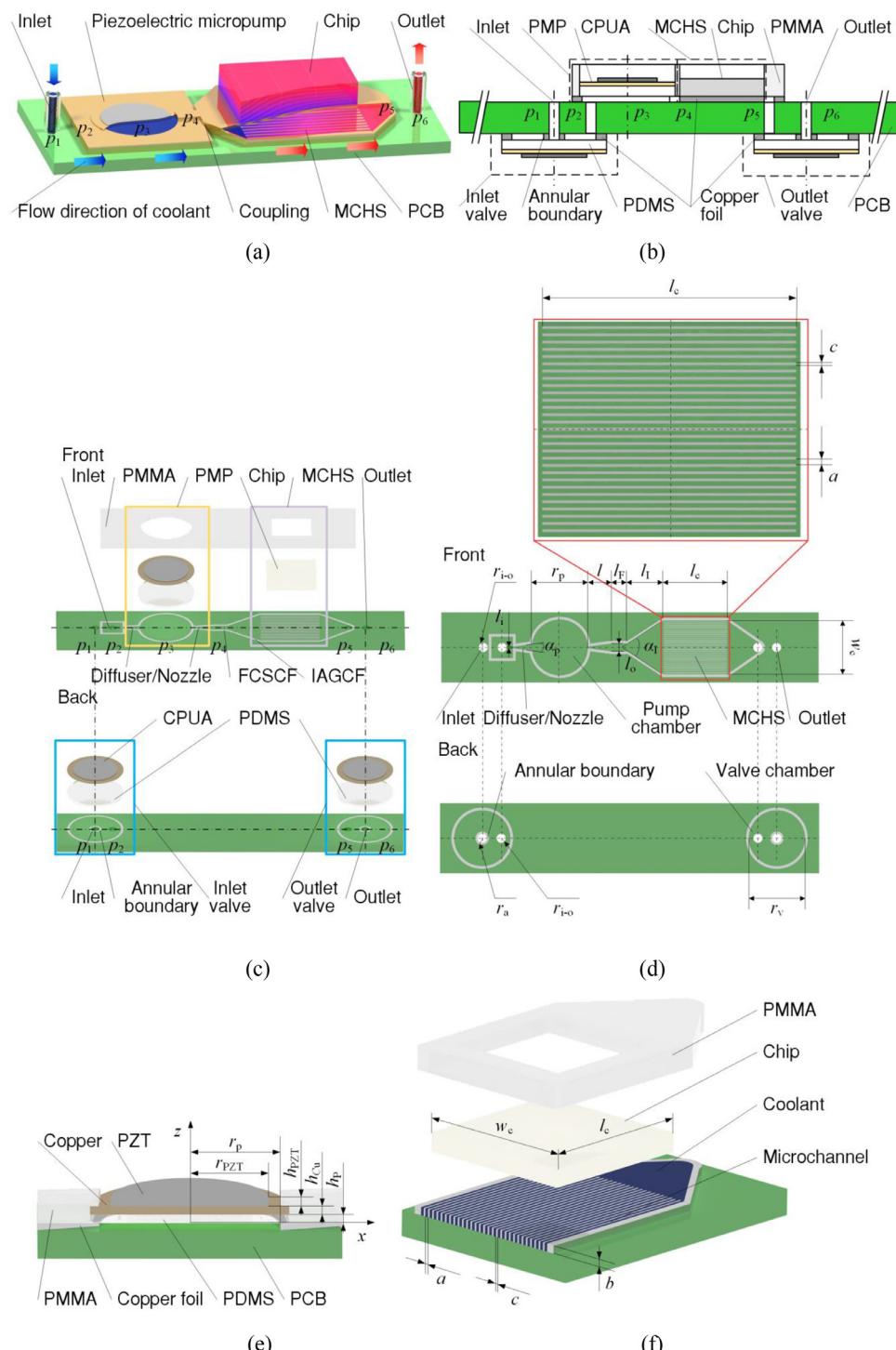


Fig. 1. Cooling chip by EAMCHS integrated on PCB (p_1 to p_6 represent the pressures at inlet of EAMCHS, inlet of PMP, chamber of PMP, outlet of PMP or inlet of MCHS, outlet of MCHS and outlet of EAMCHS, respectively): (a) 3D integration principle, (b) 2D structural principle, (c) 3D exploded drawing, (d) PCB substrate of EAMCHS, (e) the sectional view of PMP of EAMCHS and (f) 3D exploded drawing of MCHS with chip to be cooled.

Table 1
Geometrical parameters of EAMCHS (Unit: mm except for α_p and α_c).

Number	Symbol	value	Number	Symbol	value	Number	Symbol	value
1	a	0.21	8	l_F	3	14	r_p	5.2
2	b	0.105	9	l_I	6.751	15	r_{PZT}	4.5
3	c	0.127	10	l_c	10	16	r_v	5.2
4	h_{PZT}	0.1	11	l_i	0.3	17	w_c	10
5	h_{Cu}	0.11	12	l_o	1.928	18	α_p	15°
6	h_{PDMS}	0.5	13	r_a	1.25	19	α_I	33°
7	l	3.537	14	r_{i-o}	0.85			

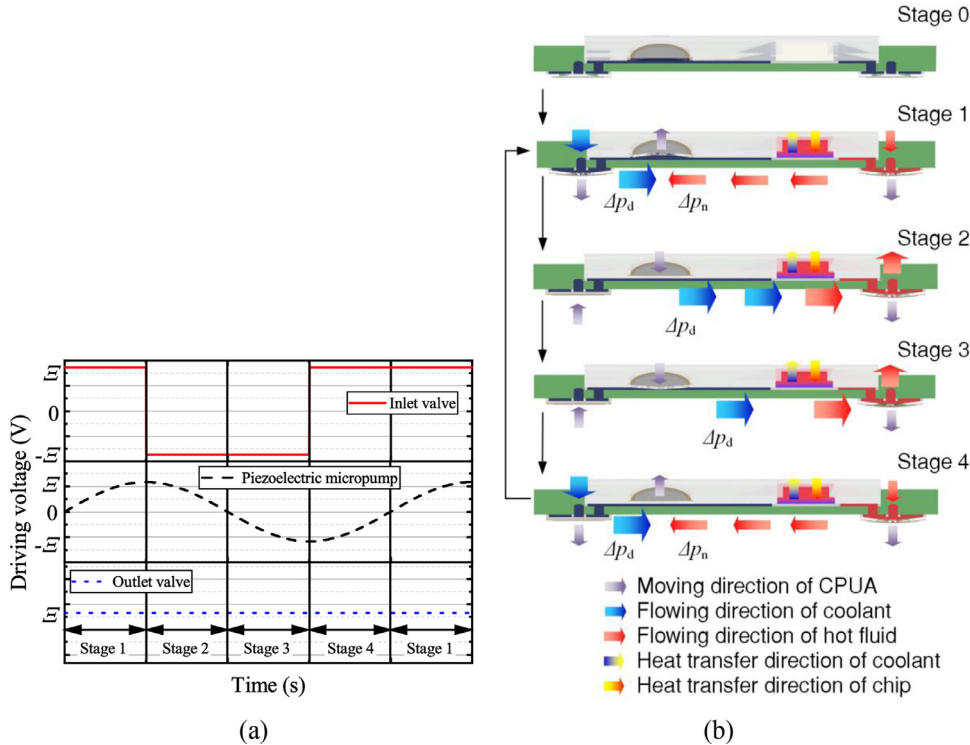


Fig. 2. Working processes of cooling chip on PCB by EAMCHS: (a) driving voltages and (b) working processes.

mized according to [34,35] and the piezoelectric microvalve is designed and optimized according to [33].

2.2. Working processes

Fig. 2 illustrates the working processes of cooling chip on PCB by EAMCHS. From Fig. 2(a), driving voltages action on CPUAs of inlet valve, PMP and outlet valve are set to square wave, sinusoidal wave and direct current (DC), respectively. Fig. 2(b) shows the corresponding working processes. From Fig. 2, when EAMCHS works, outlet valve works in the normally open state, inlet valve and PMP work in the periodic working state. Therefore, fluid driving module of EAMCHS can continuously transport the coolant to chip cooling module, and the purpose of EAMCHS to active heat dissipation of chip is realized. From Fig. 2(b), the working processes of EAMCHS are as follows: 1) stage 0, EAMCHS is in standby mode; 2) stage 1, EAMCHS starts to work under the action of driving voltages, inlet and outlet valves are opened, PMP produces differential pressure of Δp_d and Δp_n at its inlet and outlet, respectively. In this way, outside coolant is sucked in pump chamber under the action of Δp_d , and coolant inside MCHS is sucked in pump chamber under the action of Δp_n ; 3) stage 2, inlet valve is closed, outlet valve remains open, PMP produces differential pressure of Δp_n at its outlet. In this way, coolant is discharged from pump chamber to MCHS under the action of Δp_n . Meanwhile, coolant begins to transfer heat with chip in MCHS, and EAMCHS starts cooling the chip; 4) stage 3, inlet valve remains closed, outlet valve remains open, PMP produces differential pressure of Δp_n at its outlet. In this way, PMP is continuously discharged coolant from pump chamber to MCHS under the action of Δp_n . Meanwhile, coolant continuously transfers heat with chip in MCHS, and EAMCHS continuously cools the chip; 5) stage 4, inlet valve is opened, outlet valve remains open, PMP produces differential pressure of Δp_d and Δp_n at its inlet and outlet, respectively. In this way, outside coolant is sucked in pump chamber under the action of Δp_d , and coolant inside MCHS is sucked in pump chamber under the ac-

tion of Δp_n . By allowing EAMCHS to work cyclically in stages 1 to 4, it can realize continuous pumping of coolant, continuous thermal management of chip and active control of its heat dissipation performance.

From Fig. 2, the reasons for inlet valve to work periodically and outlet valve to keep open are as follows: 1) PMP can suck coolant from inlet and outlet at the same time, so as to improve suction efficiency of coolant, reduce the required time to suck the same volume of coolant and improve working efficiency of EAMCHS; 2) PMP can only discharge coolant towards the direction of outlet to improve output flow rate and reduce the loss of flow rate, so that more coolant can enter chip cooling module for heat dissipation of chip, so as to improve heat transfer capacity of EAMCHS.

2.3. Manufacturing processes

Fig. 3(a) and 3(b) show the photographs of manufactured PCB substrate of EAMCHS which is according to the geometrical parameters of EAMCHS listed in Table 1. The thickness of PCB and copper foil layer on the top and bottom layers of PCB are 800 μm and 105 μm , respectively. Fig. 3(c) to 3(e) show the photographs of the assembly processes of EAMCHS, including assembling HTCC. The assembly processes are as follows: 1) fixing PDMS coaxially on the chamber walls of inlet valve, PMP and outlet valve on PCB substrate, and then fixing CPUA coaxially on PDMS, 2) installing HTCC to simulate chip heating directly on MCHS, 3) installing PMMA on the top front side of the PCB substrate of EAMCHS and 4) installing fluid tubes of inlet and outlet and sub-miniature-A (SMA) connector on the PCB substrate of EAMCHS, and connecting CPUA to SMA connector by the copper wire.

From Fig. 3, according to the proposed principle and structure of cooling chip on PCB by EAMCHS, using existing PCB process, the embedded integration of PMP and MCHS on PCB can be realized perfectly, so as to manufacture EAMCHS with high accuracy. Moreover, the size and weight of the assembled EAMCHS are small (about 6.5 cm^3) and light (about 18.2 g), respectively.

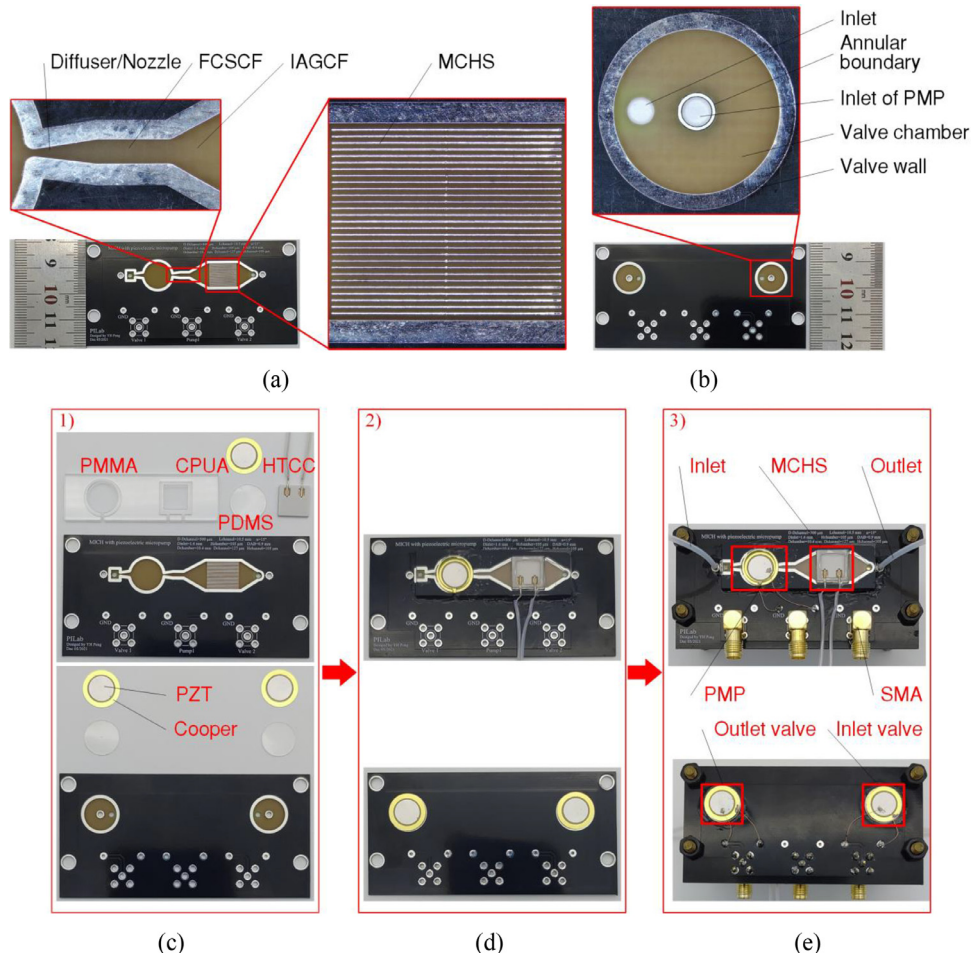


Fig. 3. Photographs of EAMCHS: (a) the front side of the manufactured PCB substrate, (b) the back side of the manufactured PCB substrate, (c) before assembly, (d) during assembly including the processes (1), (2) and (3) and (e) after assembly.

3. Finite element simulation and analysis

In this section, utilizing the COMSOL multiphysicsTM, the characteristics of the flow and heat transfer of cooling chip on PCB by EAMCHS are modeled, simulated and analyzed with FEM. During the simulation processes, the physical fields used include piezoelectric devices, fluid-solid coupling and conjugated heat transfer-laminar flow. Among them, piezoelectric devices are used to simulate the deformation and stress of CPUA due to the inverse piezoelectric effect under the action of driving voltage, the fluid-solid coupling is used to simulate the interaction between coolant and CPUA and between MCHS and chip in the processes of PMP pumping coolant, and conjugated heat transfer-laminar flow is used to simulate heat transfer between MCHS and chip. Moreover, all the governing equations used in the simulation are automatically generated by the software according to the selected physical fields and research content.

To simplify the finite element simulation and ensure it to converge, the assumptions are made as follows: 1) when establishing the finite element simulation model of cooling chip by EAMCHS, the interactions between coolant and CPUA and between MCHS and chip are directly simulated by ignoring the existence of PCB, 2) the inlet and outlet valves operate in good conditions to flow the coolant from inlet to outlet without backflow and 3) the coolant is an incompressible fluid and is in laminar flow state. Based on the above assumptions, the existence of inlet and outlet valves can

be ignored in finite element simulation model. In the selection of boundary layer, the inlet and outlet are set rather than to an open boundary. Moreover, in the finite element simulation, the ambient temperature is set to 15 °C

Fig. 4 shows the finite element simulation model and meshing results of cooling chip by EAMCHS. From Fig. 4, it can be seen that materials added to the finite element simulation model of cooling chip by EAMCHS include water, PDMS, PZT-5H, copper and silicon. The material of chip to be cooled is set to silicon. In the mesh generation of model, the mesh of the fluid part is defined as moving mesh to predefine finer meshes with the element size calibrated by fluid dynamics. The meshes of the solid parts are divided by regular meshes with the element size calibrated by general physical quantities. Meanwhile, since the MCHS has a total of thirty channels, the first channel ($i = 1$) defining the MCHS is located at the top and numbered in turn. The geometric parameters of finite element simulation model of cooling chip by EAMCHS are listed in Table 1, the working state parameters are listed in Table 2 and the driving voltage is a sinusoidal signal. To ensure the convergence of finite element simulation, simulation processes are as follows: 1) transient finite element simulations of the two physical fields (including piezoelectric devices and fluid-solid interaction) of cooling chip by EAMCHS are carried out to obtain the average flow velocity of the coolant at the inlet of MCHS and 2) steady state finite element simulations are performed on the two physical fields (including fluid-solid interaction and conjugate heat transfer-laminar

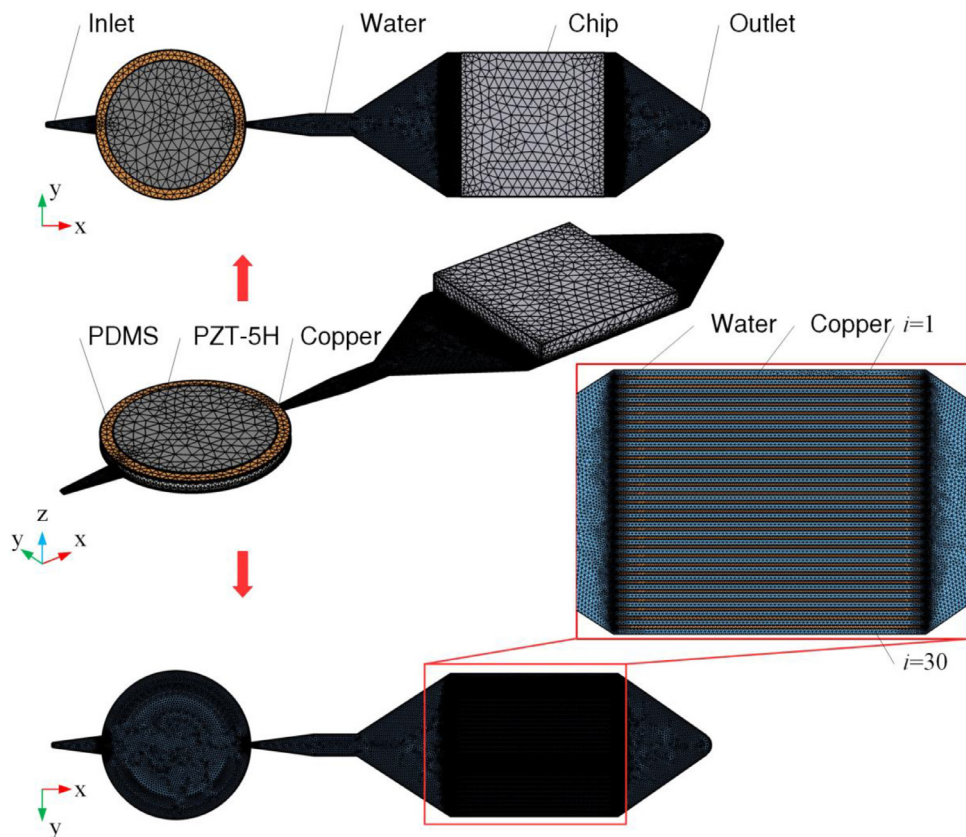


Fig. 4. Finite element simulation model and meshing results of cooling chip by EAMCHS with coupling of FCSCF, IAGCF and chip to be cooled.

Table 2

Working state parameters of cooling chip by EAMCHS.

Number	Parameter	Symbol	Value
1	Amplitude of sinusoidal driving voltage (V)	-	50
2	Frequency of sinusoidal driving voltage (Hz)	-	1200
3	Initial temperature of coolant (°C)	t_{in}	15
4	Input pressure at inlet (Pa)	p_i	0
5	Input pressure at outlet (Pa)	p_o	0
6	Chip power (W)	Q	50

flow) of cooling chip by EAMCHS, and by using the average flow rate obtained from 1) as the flow velocity of coolant at the inlet of MCHS, the flow velocity distribution inside EAMCHS and temperature distribution of chip in steady state are obtained. In the finite element simulation model, water is set to incompressible fluid, copper and PDMS are set to solid, chip is set to solid and heat source and PZT-5H is set to solid and piezoelectric devices, then, the governing equations will be automatically generated by COM-SOL Multiphysics™ and added into the finite element simulation model.

3.1. Grid independence test

To ensure the accuracy of finite element simulation and reduce the calculation time, five grids with different sizes are considered for grid independence test. Table 3 lists the maximum temperature of cooling chip and normalized calculation time obtained by FEM under the working parameters which are listed in Table 2. From Table 3, after the number of grid points reached 1,118,740, the variation of finite element simulation results is not very obvious. By comparing the simulation results, and combining the accu-

racy and calculation time, the number of grid points is chosen to be 1,118,740.

3.2. Results and discussions

Fig. 5(a) and 5(b) show the finite element simulation results of working processes of cooling chip by EAMCHS when the CPUA of PMP moves up and down to the maximum position, respectively. From Fig. 5, CPUA arches upward and downward alternately under the action of driving voltage to change the volume of the pump chamber, then it changes the pressure to drive the flow of coolant in EAMCHS. According to the simulation results, under the driving voltage with amplitude of 50 V and frequency of 1200 Hz, the maximum upward and downward center deflection of CPUA are 8.46 μm and -8.88 μm , respectively. It also can be seen from Figs. 5(a) and 5(b), the chip mounted on the MCHS is shown in green, indicating that it does not shift during the operation of cooling chip by EAMCHS.

Fig. 6(a) shows the finite element simulation results of the distribution of the flow velocity field inside EAMCHS when the heat flux of chip is 50 W/cm² and the amplitude and the frequency of driving voltage are 50 V and 1200 Hz, respectively. Fig. 6(b) shows the distribution of the flow velocity field inside EAMCHS at different positions in each channel of MCHS. From Fig. 6(a), in this case, the maximum flow velocity of coolant in the EAMCHS is 0.8 m/s at the diffuser/nozzle of PMP. Due to the diffuser/nozzle of PMP, the flow area of the coolant here will suddenly decrease. Therefore, when the flow rate remains unchanged, the flow velocity of the coolant is much higher than that in MCHS. Moreover, the coolant inside EAMCHS can flow fully uniformly inside MCHS after flowing out of PMP, and its distribution of the flow velocity is uniform inside MCHS. From Fig. 6(b), the coolant has the fastest flow velocity inside the 15th channel and the slowest inside the 30th

Table 3
Grid independence test.

Number	Number of grid points	Maximum temperature of cooling chip (°C)	Normalized calculation time
1	244,749	61.2	0.038
2	516,614	60.3	0.068
3	1,118,740	59.4	0.131
4	2,459,444	59.2	0.311
5	6,024,464	59.1	1

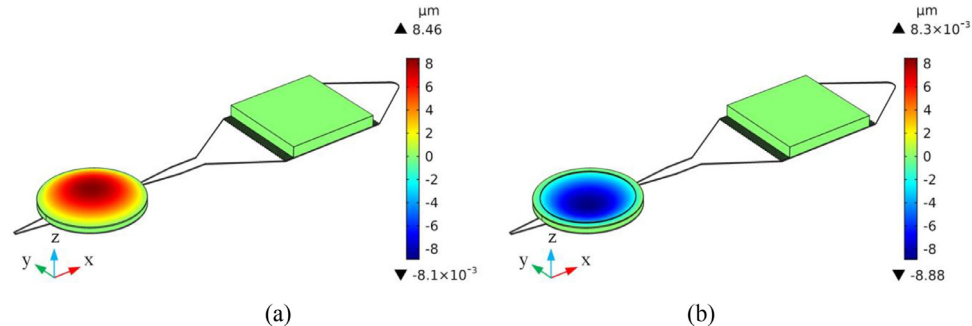


Fig. 5. Finite element simulation results of the working processes of CPUA on EAMCHS with coupling of FCSCF and IAGCF: (a) up and (b) down.

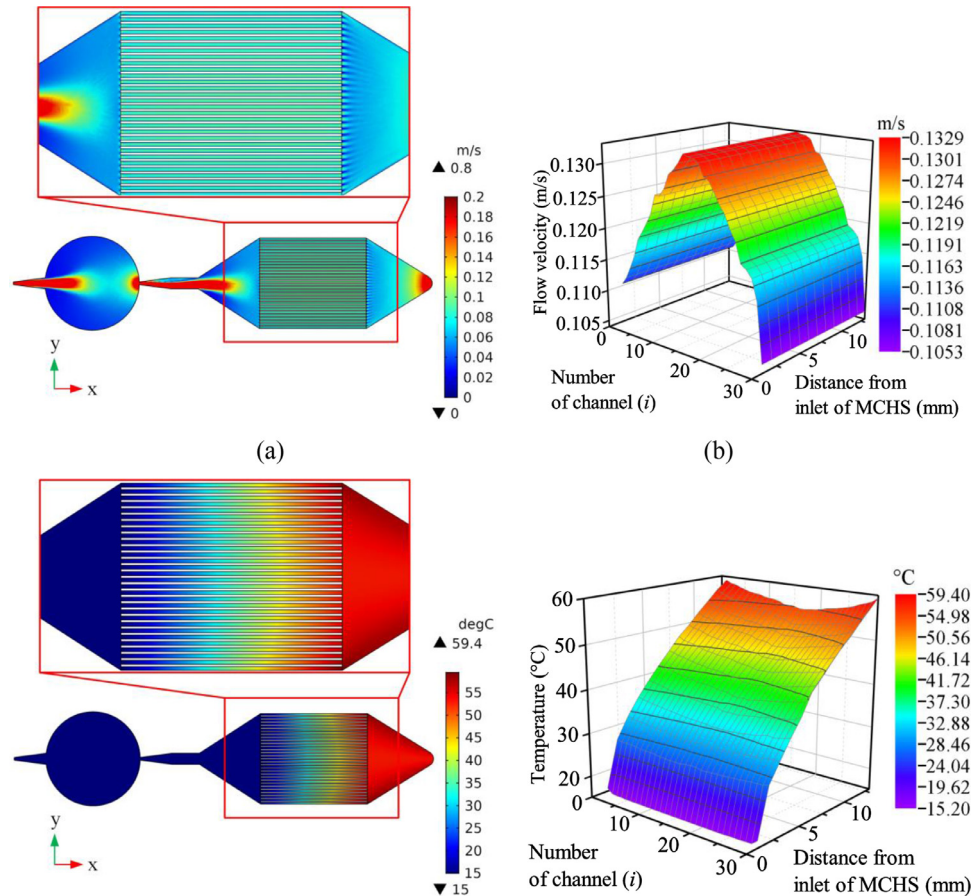


Fig. 6. Finite element simulation results of cooling chip by EAMCHS with coupling of FCSCF and IAGCF: (a) distribution of flow velocity field (after adjusting the display range of color legend), (b) flow velocity along different channels, (c) distribution of temperature field and (d) temperature along different channels.

channel. The difference between them is only 0.0276 m/s. It is indicated that the coolant can flow uniformly inside the MCHS to achieve uniform heat dissipation for the chip. Therefore, EAMCHS with coupling of FCSCF and IAGCF in series has excellent working performance. It is noted that in order to observe the flow veloc-

ity field distribution of coolant inside MCHS, the display range of color legend is adjusted. Fig. 6(c) shows the finite element simulation results of the temperature field distribution inside EAMCHS when the heat flux of chip is 50 W/cm² and the amplitude and the frequency of driving voltage are 50 V and 1200 Hz, re-

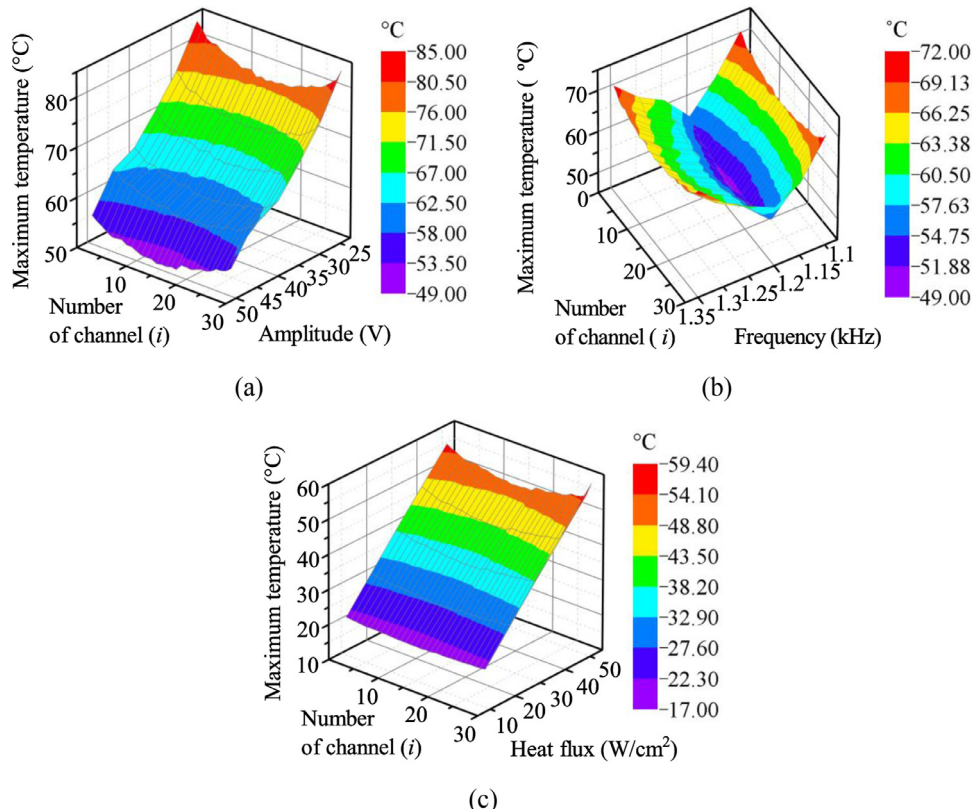


Fig. 7. The maximum temperature of each channel in MCHS of cooling chip by EAMCHS with coupling of FCSCF and IAGCF obtained by FEM: (a) when the amplitude of the driving voltage on CPUA changes, (b) when the frequency of the driving voltage on CPUA changes and (c) when the heat flux of chip changes.

spectively. Fig. 6(d) shows the distribution of temperature field inside EAMCHS at different positions in each channel of MCHS. From Fig. 6(c) and 6(d), the temperature field inside MCHS is uniformly distributed at the same position in different channels of MCHS, and the temperature field distribution at different positions in the same channel increases with the increase of the distance from the inlet of MCHS. The longer distance of coolant in MCHS flows, the more heat exchange between coolant and chip is, and the more obvious temperature rise of coolant has. The maximum temperature of chip is 59.4 °C. Therefore, EAMCHS with coupling of FCSCF and IAGCF in series has excellent heat dissipation performance.

Fig. 7(a) shows the relationship between the maximum temperature of each channel in MCHS of cooling chip by EAMCHS and the amplitude of the driving voltage applied to CPUA obtained by FEM when the frequency of the driving voltage is 1200 Hz and the heat flux of chip is 50 W/cm^2 . From Fig. 7(a), the temperature of the coolant in MCHS decreases with increasing the amplitude of the driving voltage. This is because the larger the amplitude of the driving voltage is, the larger the central deflection of CPUA is, resulting in the larger the output flow rate of PMP is, and the stronger the heat dissipation performance of EAMCHS is. Therefore, by changing amplitude of the driving voltage, the EAMCHS can achieve the active control of heat dissipation. Meanwhile, with increasing the amplitude of the driving voltage, the nonuniformity of the temperature distribution of the coolant inside MCHS of EAMCHS does not change basically. Moreover, when the amplitude of the driving voltage is 50 V, the temperature difference of the coolant inside MCHS of EAMCHS reached the maximum of 5.01 °C. The results show that EAMCHS with coupling of FCSCF and IAGCF in series has excellent heat dissipation performance. Fig. 7(b) shows the relationship between the maximum temperature of each channel in MCHS of cooling chip by EAMCHS and the frequency of the driving voltage applied to CPUA obtained

by FEM when the amplitude of the driving voltage is 50 V and the heat flux of chip is 50 W/cm^2 . From Fig. 7(b), the temperature of the coolant inside MCHS first decreases and then increases with increasing the frequency of the driving voltage, and the lowest temperature occurs when the frequency is 1200 Hz. This is because the closer the PMP works to its optimal working frequency, resulting in the greater its output flow rate is, and the stronger heat dissipation performance of EAMCHS is. Therefore, the optimal working frequency of EAMCHS is 1200 Hz. Therefore, by changing the frequency of the driving voltage, the EAMCHS can achieve the active control of heat dissipation. Meanwhile, with increasing the frequency, the nonuniformity of the temperature distribution of the coolant inside MCHS of EAMCHS does not change basically. Moreover, when the frequency of the driving voltage is 1200 Hz, the temperature difference of the coolant inside MCHS of EAMCHS reached the maximum of 5.01 °C. The results show that EAMCHS with coupling of FCSCF and IAGCF in series has excellent heat dissipation performance. Fig. 7(c) shows the relationship between the maximum temperature of each channel in MCHS of cooling chip by EAMCHS and the heat flux of chip obtained by FEM when the amplitude and frequency of the driving voltage are 50 V and 1200 Hz, respectively. From Fig. 7(c), the temperature distribution of the coolant is uniform inside MCHS and that hardly changes with the change of heat flux of chip. Moreover, when the heat flux of chip is 50 W/cm^2 , the temperature difference of the coolant inside MCHS of EAMCHS reached the maximum of 5.01 °C. The results show that EAMCHS with coupling of FCSCF and IAGCF in series has excellent heat dissipation performance.

4. Theoretical modeling and simulation

According to the structural principle of cooling chip on PCB by EAMCHS shown in Fig. 1, the heat transfer characteristics and

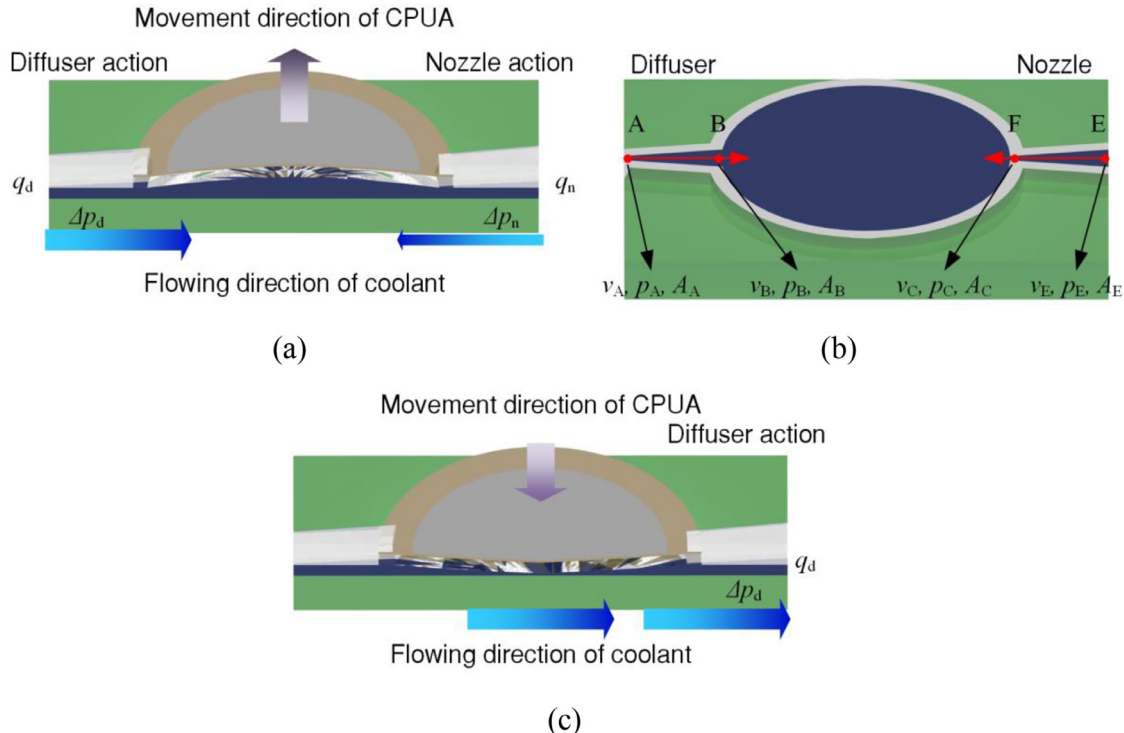


Fig. 8. Structural principle of PMP of fluid driving module: (a) coolant suction, (b) different points on same streamline at diffuser and nozzle when PMP sucks coolant and (c) coolant discharging.

flow characteristics of cooling chip on PCB by EAMCHS are analyzed through establishing the flow rate model and heat transfer model. The modeling processes are as follows: 1) according to frictional drag equation, local resistance equation, Bernoulli's principle and continuity equation, the flow rate model of EAMCHS is established to obtain the output flow rate q_{p-c} , the flow rate q_c in each channel of MCHS can be calculated through q_{p-c} , and 2) according to Fourier's first law, Newton's law of cooling and Sieder-Tate equation, the heat transfer model of EAMCHS is established, and the temperature of the chip in steady state after heat dissipation through the MCHS is obtained.

4.1. Modeling flow rate

Fig. 8(a) to 8(c) show schematic diagram of coolant suction of PMP, different points on same streamline at diffuser and nozzle of PMP when it sucks coolant and schematic diagram of coolant discharging of PMP, respectively. According to Bernoulli's principle, Fig. 8(a) and 8(b), the relationship between different two points on same streamline at diffuser can be expressed as

$$\frac{1}{2}\rho_l v_A^2 + p_A = \frac{1}{2}\rho_l v_B^2 + p_B \quad (1)$$

where ρ_l is the density of coolant, v is the flow velocity of coolant, p is the pressure, subscripts A and B represent any different two points on the same streamline at diffuser.

Therefore, the differential pressure in diffuser can be expressed as

$$\Delta p_d = -\frac{1}{2}\rho_l v_A^2 \left(1 - \frac{A_A^2}{A_B^2}\right) = \xi_d \left(\frac{\rho_l v_A^2}{2}\right) \quad (2)$$

where A_A is the cross-sectional area of coolant at point A, A_B is the cross-sectional area of coolant at point B and ξ_d is the local damping coefficient of diffuser.

Similarly, the differential pressure in nozzle can be expressed as

$$\Delta p_n = \frac{1}{2}\rho_l v_F^2 \left(1 - \frac{A_F^2}{A_E^2}\right) = \xi_n \left(\frac{\rho_l v_F^2}{2}\right) \quad (3)$$

where v_F is the flow velocity of coolant at point F, A_F is the cross-sectional area of coolant at point F, A_E is the cross-sectional area of coolant at point E and ξ_n is the local damping coefficient of nozzle.

Then, according to continuity equation, we have

$$q_d = A_d \left(\frac{2}{\rho_l}\right)^{\frac{1}{2}} \left(\frac{\Delta p_d}{\xi_d}\right)^{\frac{1}{2}} \quad (4)$$

$$q_n = A_n \left(\frac{2}{\rho_l}\right)^{\frac{1}{2}} \left(\frac{\Delta p_n}{\xi_n}\right)^{\frac{1}{2}} \quad (5)$$

where q_d and q_n are the flow rate at diffuser and nozzle, respectively; A_d and A_n are the cross-sectional areas of inlet of diffuser and nozzle, respectively; v_d and v_n are the flow velocity at the cross-sectional area of inlet of diffuser and nozzle, respectively.

The relationship between the flow rate at inlet and outlet of PMP can be expressed as

$$q_{in} - q_{out} = \frac{dV_t}{dt} \quad (6)$$

where q_{in} and q_{out} are the flow rate at inlet and outlet of PMP, respectively; V_t is the volume change of PMP, and according to [36], it can be expressed as

$$V_t = \frac{\pi}{3}w(r)|_{r=0}r_p^2 \sin(2\pi ft) \quad (7)$$

where r_p is the radius of pump chamber, $w(r)|_{r=0}$ is the central deflection of CPUA and subscript $|_{r=0}$ represents the central position of CPUA, f is the frequency of driving voltage.

According to Section 2.2, the coolant suction and discharging of PMP follow the following rules: 1) when sucking coolant, the

diffuser and nozzle of PMP suck coolant at the same time; 2) when discharging coolant, only the diffuser of PMP discharges coolant. Based on these rules, flow rate at outlet of PMP can be established as follows:

a) Flow rate at outlet of PMP when it sucks coolant

From Fig. 8(a), when PMP sucks coolant, flow rate at inlet and outlet can be expressed as

$$\begin{cases} q_{in} = q_d \\ q_{out} = -q_n \end{cases} \quad (8)$$

According to [34] and [35] and Eqs. (4), (5) and (8), flow rate at outlet of PMP can be obtained as

$$\dot{q}_{out} = -q_n = -\frac{\frac{2\pi^2}{3}w(r)|_{r=0}r_p^2f\cos(2\pi ft)}{1 + \sqrt{\frac{\zeta_n}{\zeta_d}}} \quad (9)$$

b) Flow rate at outlet of PMP when it discharges coolant

From Fig. 8(c), when PMP discharges coolant, flow rate at inlet and outlet can be expressed as

$$\begin{cases} q_{in} = 0 \\ q_{out} = q_d \end{cases} \quad (10)$$

According to [34] and [35] and Eqs. (4), (5) and (8), flow rate at outlet of PMP can be expressed as

$$\dot{q}_{out} = q_d = -\frac{\frac{2\pi^2}{3}w(r)|_{r=0}r_p^2f\cos(2\pi ft)}{1 + \sqrt{\frac{\zeta_d}{\zeta_n}}} \quad (11)$$

Accordingly, when PMP works for one cycle of T , its total flow rate can be expressed as

$$q_{p-c} = \frac{V}{T} = \frac{1}{T} \left(\int_{\frac{T}{4}}^{\frac{3T}{4}} \ddot{q}_{out} dt + \int_{-\frac{T}{4}}^{\frac{T}{4}} \dot{q}_{out} dt \right) \quad (12)$$

where V is the total volume change of PMP when it works for one cycle.

Eq. (12) can be rewritten as

$$q_{p-c} = \frac{\frac{2\pi}{3}w(r)|_{r=0}r_p^2}{T} \left[\frac{\frac{\zeta_n}{\zeta_d} - 1}{2\sqrt{\frac{\zeta_n}{\zeta_d} + \frac{\zeta_n}{\zeta_d} + 1}} \right] \quad (13)$$

Eq. (13) is the established flow rate model of fluid driving module in EAMCHS.

c) Flow rate in each channel of MCHS

Considering that the coolant can flow uniformly in each channel of the MCHS and according to continuity equation, we have

$$nq_c = q_{p-c} \quad (14)$$

where n is the number of channels of MCHS and q_c is the flow rate of coolant in one channel.

According to Eq. (14), the flow velocity of coolant in one channel can also be obtained as

$$v_c = \frac{q_{p-c}}{nA} \quad (15)$$

where A is the cross-sectional area of one channel.

4.2. Modeling heat transfer

According to Fig. 1(f), in process of establishing the heat transfer model of chip cooling module, it is assumed that the coolant is fully developed laminar flow. The Reynolds number of coolant flowing in each channel can be expressed as

$$Re = \frac{\rho_l v_c d_h}{\mu_{in}} \quad (16)$$

where μ_{in} is the viscosity of coolant at inlet of MCHS and d_h is the hydraulic diameter of each microchannel.

Sieder-Tate [37] is used to calculate the Nusselt coefficient of MCHS, which can be expressed as

$$Nu = 1.86 \left(\frac{Re Pr_{in} d_h}{l_c} \right)^{\frac{1}{3}} \quad (17)$$

where Pr_{in} is the Prandtl number of coolant at inlet of MCHS.

Therefore, the surface heat transfer coefficient of coolant in each channel can be expressed as

$$h = \frac{Nu \lambda_{in}}{d_h} \quad (18)$$

where λ_{in} is the thermal conductivity of coolant at inlet of MCHS.

Considering the heat transfer coefficient h up the walls and the modeling heat flow in the walls as one-dimensional, the efficiency of MCHS can be expressed as

$$\eta = \frac{\tanh N}{N} \quad (19)$$

N in Eq. (19) can be expressed as

$$N = \sqrt{\frac{2h}{\lambda_w c}} b \quad (20)$$

where λ_w is the thermal conductivity of MCHS wall.

According to [2], the convective thermal resistance and heat transfer resistance of MCHS can be obtained as

$$R_{conv} = \frac{d_h}{\lambda_{in} Nu w_c l_c \alpha \eta} \quad (21)$$

$$R_{heat} = \frac{1}{\rho_l q_{p-c} c_p} \quad (22)$$

where c_p is the specific heat of coolant and α is the surface area multiplication factor.

Therefore, when the chip power is Q , the temperature differences of thermal convection and heat conduction of coolant can be expressed as

$$\Delta t_{conv} = QR_{conv} \quad (23)$$

$$\Delta t_{heat} = QR_{heat} \quad (24)$$

Under the action of temperature difference of heat conduction of coolant, the temperature rise of chip can be obtained as

$$\Delta t_{chip} = \frac{Q}{2nh l_c (a+b)} \quad (25)$$

According to the logarithmic average temperature difference, the temperature rise of chip under the action of heat conduction of coolant can also be obtained as

$$\Delta t_{chip} = \frac{\Delta t_{heat}}{\ln \frac{t_{heat} - t_{in}}{t_{heat} - t_{in} - \Delta t_{heat}}} \quad (26)$$

where t_{in} is the temperature of coolant at inlet, Δt_{heat} is the temperature of chip under the action of heat conduction of coolant.

Eq. (26) can be rewritten as

$$t_{heat} = \Delta t_{heat} + t_{in} + \frac{\Delta t_{heat}}{e^{\frac{\Delta t_{heat}}{\Delta t_{chip}}} - 1} \quad (27)$$

Therefore, when chip operates in steady state, the actual temperature can be expressed as

$$t_{chip} = t_{heat} + \Delta t_{conv} \quad (28)$$

Eq. (28) is the established heat transfer model of chip cooling module in EAMCHS.

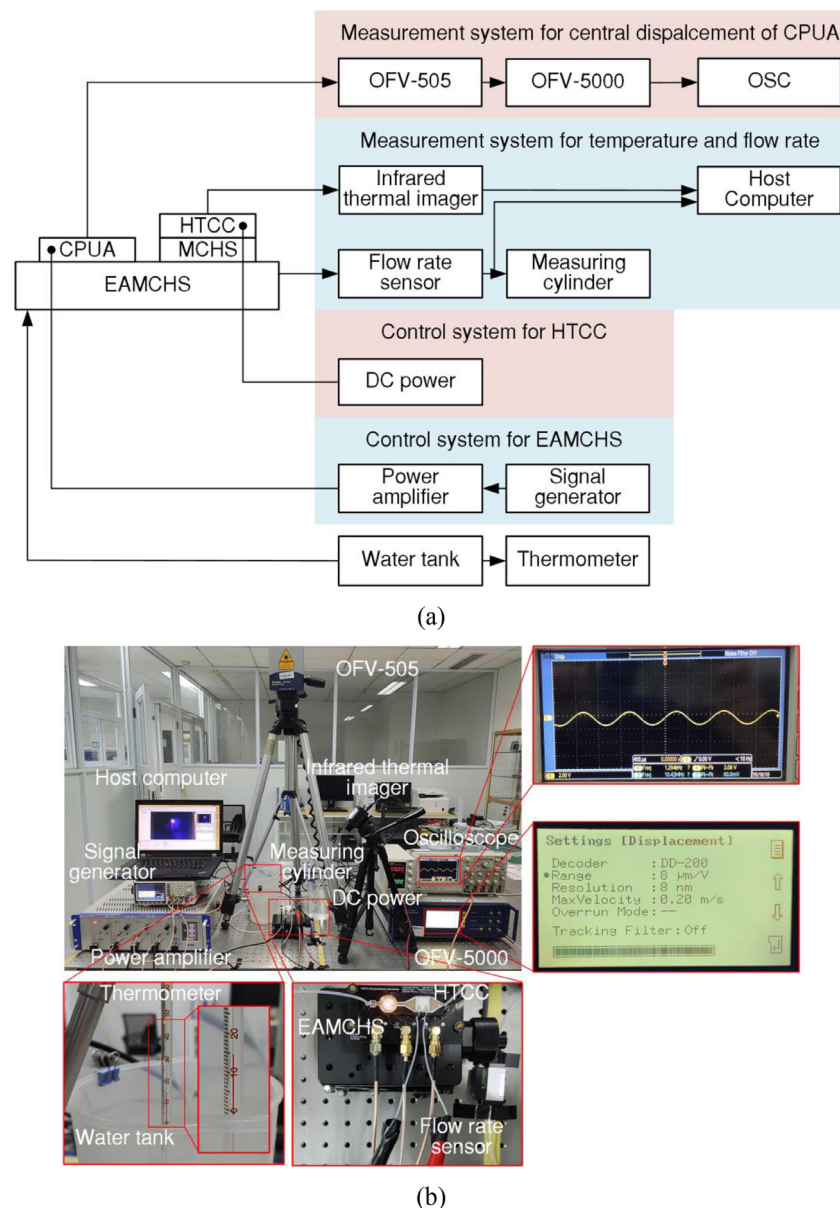


Fig. 9. Experimental setup: (a) schematic diagram and (b) photograph.

5. Experiments and discussions

5.1. Experimental setup

Fig. 9(a) and 9(b) illustrate the schematic diagram and photograph of experimental setup of cooling chip on PCB by EAMCHS, respectively. In experiment, HTCC with the maximum heat flux of 50 W/cm^2 are used to simulate chip heating. From Fig. 9, the experimental setup is mainly composed of control systems for EAMCHS and HTCC, and measurement systems for central deflection of CPUA, temperature and flow rate. The control system for EAMCHS, which controls the working state of fluid driving module to realize the purpose of controlling flow rate of EAMCHS, is mainly composed of a multi-channel piezoelectric ceramic power amplifier (model: AMP-304.03.A.150, DH Science & Technology Co. Ltd, China) and a multi-channel signal generator (model: MFG 2260MRA, Good Will Instrument Co. Ltd, China). The control system for HTCC, which controls the power of HTCC, is mainly composed of a DC power (model: UTP3315TFL-II, Uni-Trend Technology Co., Ltd., China).

The measurement system for the central deflection of CPUA, which measures the central deflection $w(r)|_{r=0}$ of CPUA on PMP is mainly composed of a laser Doppler vibrometer (LDV, model: OFV-505/5000, Polytec GmbH, Germany) and an oscilloscope (model: DPO 2014B, Tektronix Inc., USA). The measurement system for temperature and flow rate, which measures the temperature of HTCC and the flow rate of EAMCHS, is mainly composed of an infrared thermal imager (model: A65, Teledyne FLIR, USA), a flow rate sensor (model: SLS-1500, Sensirion AG, Switzerland), a measuring cylinder and a host computer. Meanwhile, a thermometer is used to measure the temperature of the coolant which is input to EAMCHS through water tank.

In experiment, the characteristics of flow and heat transfer of cooling chip on PCB by EAMCHS are tested as follows: 1) measuring the characteristics of flow and heat transfer of EAMCHS when changing the amplitude of the driving voltage, 2) measuring the characteristics of flow and heat transfer of EAMCHS when changing the frequency of the driving voltage and 3) measuring the characteristics of heat transfer of EAMCHS when changing the heat flux

Table 4
Physical parameters in numerical simulation.

Number	Parameter	Symbol	Value
1	Temperature of coolant at inlet (°C)	t_{in}	15
2	Density of coolant (kg/m ³)	ρ_l	998.95
3	Viscosity of coolant at inlet (Pa·s)	μ_{in}	0.001155
4	Prandtl number of coolant at inlet	Pr_{in}	8.27
5	Thermal conductivity of coolant at inlet (W/(m·K))	λ_{in}	0.5865
6	Thermal conductivity of MCHS wall (W/(m·K))	λ_w	111
7	Constant pressure specific heat of coolant (J/(kg·K))	c_p	4187

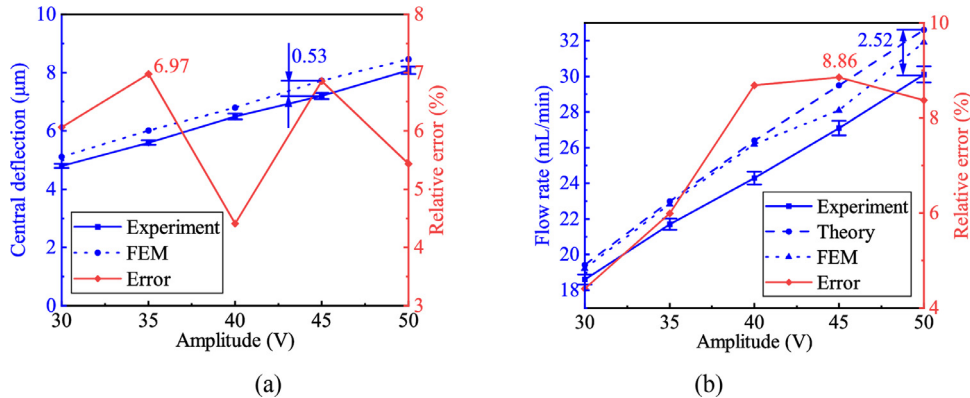


Fig. 10. Effect of the amplitude of the driving voltage on the working condition of EAMCHS: (a) the central deflection of CPUA and (b) the flow rate.

Table 5
Maximum uncertainties of primary measurements.

Number	Equipment	Measurement parameter	Value
1	OFV-505/5000	$w(r) _{r=0}$	$\pm 0.1\%$
2	SLS-1500	q_{p-c}	$\pm 0.5\%$
3	A65	t_{chip}	$\pm 0.3\ ^\circ\text{C}$

of HTCC. The phase relationship between the respective driving voltages is shown in Fig. 2(a), and their parameters are listed in Table 2. Water is used as the coolant. The temperatures obtained in experiments are steady state temperatures. When using the parameters of the driving voltage listed in Table 2, the maximum energy consumption of one piece of CPUA is 0.4 W. Therefore, the maximum energy consumption of EAMCHS driven by three pieces of CPUAs is 1.2 W. In the processes of obtaining numerical simulation results for comparison with finite element simulation results, the physical parameters in numerical simulation are listed in Table 4.

The uncertainties of the different measured parameters in the experimental error analysis are all derived from the equipments used in the experiment, and their maximum uncertainties are listed in Table 5. In order to test the repeatability of experimental measurements, ten measurements were performed for each set of experiment under the same condition, and the means of these measurements are plotted as data points at the confidence of 99.7% with the range of error bars representing the confidence intervals.

5.2. Experimental results and analysis

Fig. 10(a) depicts curves of experimental measurement and finite element simulation of the relationship between the central deflection of CPUA on PMP and the amplitude of the driving voltage, and the relative error between the experimental measurement and finite element simulation. Fig. 10(b) shows curves of experimental measurement, finite element simulation and numerical simulation of the relationship between the flow rate of EAMCHS and the amplitude of the driving voltage, and the relative error between experimental measurement and numerical simulation.

From Fig. 10(a), the central deflection of CPUA increases with increasing the amplitude, and the measured maximum central deflection is 8.08 μm when the amplitude is 50 V. The maximum deviation between experimental measurement and the finite element simulation is 0.53 μm when the amplitude is 45 V. The maximum relative error is 6.97% when the amplitude is 35 V. From Fig. 10(b), the flow rate of EAMCHS increases with increasing the amplitude, and the measured maximum flow rate is 30.11 mL/min when the amplitude is 50 V. The maximum deviation between the experimental measurement and the numerical simulation is 2.52 mL/min when the amplitude is 50 V. The maximum relative error is 8.86% when the amplitude is 45 V. According to Fig. 10 and Eq. (13), the established flow rate model of EAMCHS can accurately predict the relationship between its flow rate and the amplitude of driving voltage.

Fig. 11(a) shows the infrared thermal image of the relationship between the maximum temperature of HTCC on MCHS of EAMCHS and the amplitude of driving voltage. Fig. 11(b) shows curves of experimental measurement, finite element simulation and numerical simulation of relationship between the maximum temperature of HTCC on MCHS of EAMCHS and amplitude of driving voltage. Meanwhile, relative error curves between experimental measurement and numerical simulation are plotted simultaneously in Fig. 11(b). In this case, the heat flux of HTCC has been maintained at 50 W/cm². From Fig. 11(a), when EAMCHS works, the maximum temperature of HTCC will decrease with increasing of amplitude. Moreover, the measured maximum temperature of HTCC is 82.1 °C when the amplitude is 30 V and it decreases to 64.0 °C when the amplitude is 50 V. It shows that EAMCHS can realize the active heat dissipation and cooling of the chip, and has obvious effect, which can ensure the reliable operation of the chip. Moreover, when EAMCHS works, the maximum deviation and the maximum relative error between experimental measurement and numerical simulation are 8.35 °C and 10.76%, respectively, when the amplitude is 35 V. According to Fig. 11, EAMCHS can maximize the working performance of MCHS. Moreover, in the process of establishing the heat transfer model of EAMCHS which can be expressed as Eq. (28), it is considered that the coolant flows fully uniformly

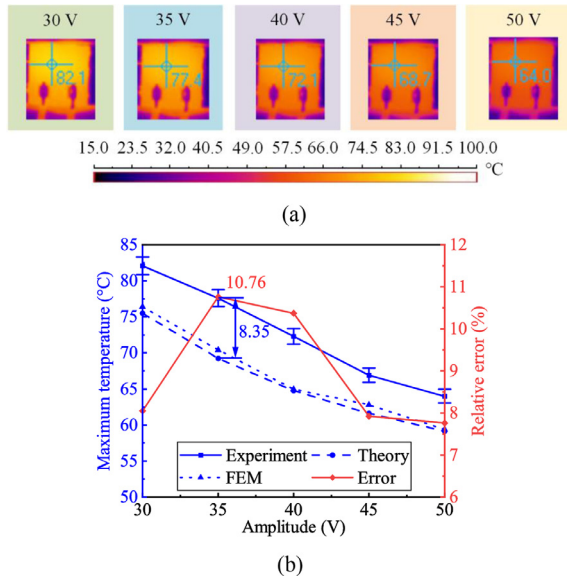


Fig. 11. Effect of the amplitude of the driving voltage on the maximum temperature of HTCC: (a) infrared thermal images and (b) curves.

in MCHS of EAMCHS. Therefore, the experimental measurement results of EAMCHS prove that the hypothesis is reasonable, and EAMCHS has excellent heat dissipation performance. Moreover, the established heat transfer model of EAMCHS can accurately predict the relationship between the temperature of chip to be cooled and the amplitude of driving voltage. From the above analysis of Fig. 11, the active control of the heat dissipation of EAMCHS can be realized and then the active chip cooling can be realized by changing the amplitude of driving voltage acting on EAMCHS.

Fig. 12(a) depicts curves of experimental measurement and finite element simulation of the relationship between central deflection of CPUA on PMP and frequency of driving voltage and the relative error between the experimental measurement and finite element simulation. Fig. 12(b) shows curves of experimental measurement, finite element simulation and numerical simulation of the relationship between flow rate of EAMCHS and frequency of driving voltage, and relative error between experimental measurement and numerical simulation. From Fig. 12(a), the central deflection of CPUA first increases and then decreases with increasing frequency, and the measured maximum central deflection is $8.08 \mu\text{m}$ when the frequency is 1200 Hz. The maximum deviation between experimental measurement and numerical simulation is $0.41 \mu\text{m}$ when the frequency is 1150 Hz. The maximum relative error between experimental measurement and numerical simulation

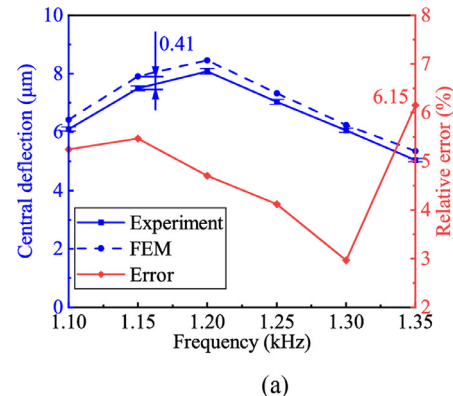


Fig. 12. Effect of the frequency of the driving voltage on the working condition of EAMCHS: (a) the central deflection of CPUA and (b) the flow rate.

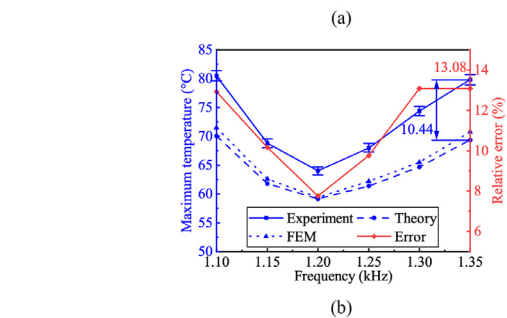
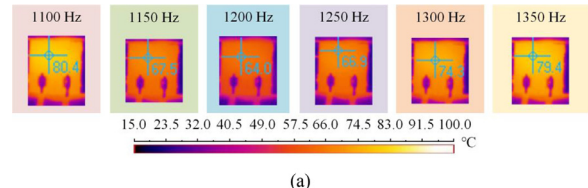
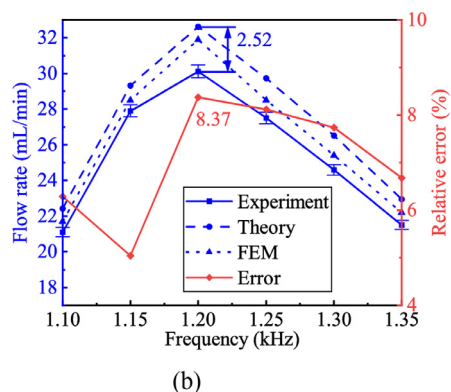


Fig. 13. Effect of the frequency of the driving voltage on the maximum temperature of HTCC: (a) infrared thermal images and (b) curves.

is 6.15% when the frequency is 1350 Hz. The closer the working frequency of CPUA is to its own natural frequency, the greater its central deflection will be. From Fig. 12(b), the flow rate of EAMCHS first increases and then decreases with increasing frequency, the measured maximum flow rate is 30.11 mL/min when the frequency is 1200 Hz, and at this frequency, the maximum deviation and the maximum relative error between experiment and numerical simulation are 2.52 mL/min and 8.37% , respectively. According to Fig. 12 and the Eq. (13), the established flow rate model of EAMCHS can accurately predict the relationship between its flow rate and frequency of driving voltage. Fig. 13(a) shows the infrared thermal image of the relationship between the maximum temperature of HTCC on MCHS of EAMCHS and the frequency of driving voltage. Fig. 13(b) shows the curves of experimental measurement, finite element simulation and numerical simulation of the relationship between the maximum temperature of HTCC on EAMCHS and frequency of driving voltage, and relative error between experimental measurement and numerical simulation. In this case, the heat flux of HTCC has been maintained at 50 W/cm^2 . From Fig. 13(a), when EAMCHS works, the maximum temperature of HTCC will first decrease and then increase with increasing of frequency. Moreover, the measured maximum temperature of HTCC is 80.4°C when frequency is 1100 Hz. From Fig. 13(b), when the frequency is 1350 Hz, the maximum deviation and the maximum relative error between experimental measurement and numerical simulation are 10.44°C and 13.08% , respectively. According to Fig. 13 and Eq. (28), EAMCHS has excellent heat dissipation performance, and it is also proved



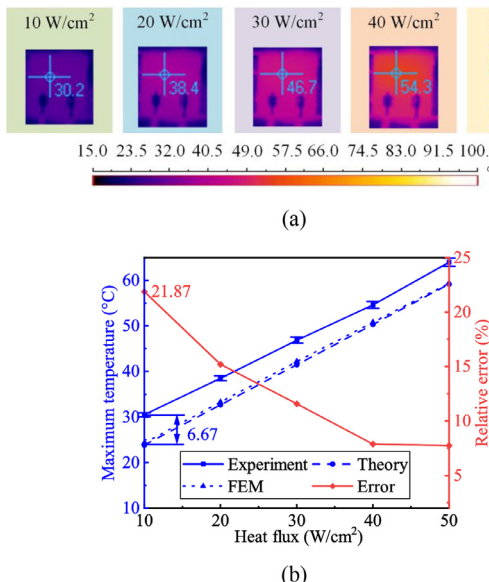


Fig. 14. Effect of heat flux of HTCC on the maximum temperature of it: (a) infrared thermal images and (b) curves.

that established heat transfer model of EAMCHS can accurately predict the relationship between the temperature of chip to be cooled and the frequency of driving voltage. From the above analysis of Fig. 13, the active control of the heat dissipation of EAMCHS can be realized and then the active cooling of the chip can be realized by changing the frequency of driving voltage acting on EAMCHS.

Fig. 14(a) shows the infrared thermal image of HTCC on MCHS of EAMCHS. Fig. 14(b) shows curves of experimental measurement, finite element simulation and numerical simulation of relationship between the maximum temperature of HTCC and its heat flux, and relative error between experimental measurement and numerical simulation. From Fig. 14(a), when EAMCHS works, the maximum temperature of HTCC will increase with increasing of its heat flux. Moreover, the measured maximum temperature of HTCC is 64.0 °C when the heat flux of HTCC is 50 W/cm². From Fig. 14(b), when the heat flux of HTCC is 10 W/cm², the maximum deviation and the maximum relative error between experimental measurement and numerical simulation are 6.67 °C and 21.87%, respectively. According to Fig. 14 and Eq. (28), EAMCHS has excellent heat dissipation performance, and it is also proved that established heat transfer model of EAMCHS can accurately predict the relationship between the temperature of chip to be cooled and its heat flux.

6. Conclusion

In this paper, the principle and structure of cooling chip on PCB by EAMCHS are proposed. EAMCHS is designed and manufactured with PCB process. The finite element simulation model and theoretical model of cooling chip on PCB by EAMCHS for active cooling chip are established to simulate and analyze the heat transfer characteristics and flow characteristics of it. An experimental setup is established to test and analyze its working performances by utilizing HTCC to simulate chip heating. The research results show that:

1) The principle and structure of cooling chip on PCB by EAMCHS can be used to active cool chip, and active cooling chip and heat dissipation performance of EAMCHS can be realized by controlling the driving voltage acting on EAMCHS. Moreover, the EAMCHS can control the temperature of HTCC at 64.0 °C with heat flux of 50 W/cm² through the flow rate of 30.11 mL/min of coolant un-

der the amplitude and frequency of driving voltage are 50 V and 1200 Hz, respectively.

2) By using the coupling of FCSCF and IAGCF in series, EAMCHS can realize the uniform flowing of coolant in MCHS to achieve uniform heat dissipation for chip, and it is proved by finite element simulation and numerical simulation.

3) Established theoretical model can describe flow characteristics and heat transfer characteristics of EAMCHS, and the maximum relative errors of flow rate and temperature of HTCC between experimental measurement and numerical simulation are 8.86% and 21.87%, respectively, which will be conducive to its structural design and optimization.

4) The EAMCHS realizes embedded integration of PMP and MCHS on PCB, which can reduce the length of fluid channel and the dosage of coolant. Moreover, the EAMCHS has low energy consumption (about 1.2 W), small size (about 6.5 cm³) and light weight (about 18.2 g), and provides a novel principle, novel method and novel structure for thermal management of chips highly integrated on PCB.

To sum up, the principle and structure of cooling chip on PCB by EAMCHS can be widely used in heat dissipation of chips on PCB. Meanwhile, cooling chip on PCB by EAMCHS can also realize active control with closed-loop feedback by adding feedback sensors.

Declaration of Competing Interest

The authors declare that they have no known competing financial interests or personal relationships that could have appeared to influence the work reported in this paper.

CRediT authorship contribution statement

Yun-Hao Peng: Methodology, Software, Validation, Data curation, Writing – original draft, Writing – review & editing. **Dai-Hua Wang:** Conceptualization, Writing – review & editing, Project administration, Visualization. **Xin-Yu Li:** Resources, Validation. **Ying Zhang:** Software, Data curation.

Data Availability

Data will be made available on request.

Acknowledgments

This work is supported by the National Natural Science Foundation of China (Grant No. U21B2074), the Advance Research Project on Civil Space Technology of State Administration of Science, Technology and Industry for National Defense, China (Grant No. D020210) and the Graduate Scientific Research and Innovation Foundation of Chongqing, China (Grant No. CYB20060).

References

- [1] Y.T. Jia, G.D. Xia, L.X. Zong, D.D. Ma, Y.X. Tang, A comparative study of experimental flow boiling heat transfer and pressure drop characteristics in porous-wall microchannel heat sink, Int. J. Heat Mass Transf. 127 (2018) 818–833.
- [2] D.B. Tuckerman, R.F.W. Pease, High-performance heat sinking for VLSI, Electron Dev. Lett. 2 (5) (1981) 126–129.
- [3] D.X. Deng, L. Zeng, W. Sun, A review on flow boiling enhancement and fabrication of enhanced microchannels of microchannel heat sinks, Int. J. Heat Mass Transf. 175 (2021) 121332.
- [4] H.A. Mohammed, G. Bhaskaran, N.H. Shuaib, R. Saidur, Heat transfer and fluid flow characteristics in microchannels heat exchanger using nanofluids: a review, Renew. Sustain. Energy Rev. 15 (3) (2011) 1502–1512.
- [5] M. Bahirei, S. Heshmatian, Electronics cooling with nanofluids: a critical review, Energy Convers. Manage. 172 (2018) 438–456.
- [6] K. Vafai, A.R.A. Khaled, Analysis of flexible microchannel heat sink systems, Int. J. Heat Mass Transf. 48 (9) (2005) 1739–1746.

- [7] D.D. Ma, G.D. Xia, W. Wang, Y.T. Jia, Y.C. Yang, Study on thermal performance of microchannel heat sinks with periodic jetting and throttling structures in sidewalls, *Appl. Therm. Eng.* 158 (2019) 113764.
- [8] G. Lu, J. Zhao, L. Lin, X.D. Wang, W.M. Yan, A new scheme for reducing pressure drop and thermal resistance simultaneously in microchannel heat sinks with wavy porous fins, *Int. J. Heat Mass Transf.* 111 (2017) 1071–1078.
- [9] D.O. Ariyo, T. Bello-Ochende, Constructal design of two-phase stacked microchannel heat exchangers for cooling at high heat flux, *Int. Commun. Heat Mass Transf.* 125 (2021) 105294.
- [10] D.D. Ma, G.D. Xia, J. Wang, Y.C. Yang, Y.T. Jia, L.X. Zong, An experimental study on hydrothermal performance of microchannel heat sinks with 4-ports and offset zigzag channels, *Energy Convers. Manage.* 152 (2017) 157–165.
- [11] A. Ebrahimi, F. Rikhtegar, A. Sabaghan, E. Roohi, Heat transfer and entropy generation in a microchannel with longitudinal vortex generators using nanofluids, *Energy* 101 (2016) 190–201.
- [12] M. Bahiraei, S. Heshmatian, Electronics cooling with nanofluids: a critical review, *Energy Convers. Manage.* 172 (2018) 438–456.
- [13] C. Anbumeenakshi, M.R. Thansekhar, On the effectiveness of a nanofluid cooled microchannel heat sink under non-uniform heating condition, *Appl. Therm. Eng.* 113 (2017) 1437–1443.
- [14] A. Sabaghan, M. Edalatpour, M.C. Moghadam, E. Roohi, H. Niazmand, Nanofluid Flow and Heat Transfer in a Microchannel with Longitudinal Vortex Generators: two-phase Numerical Simulation, *Appl. Therm. Eng.* 100 (2016) 179–189.
- [15] Y.X. Zhang, J.T. Wang, W. Liu, Z.C. Liu, Heat transfer and pressure drop characteristics of R134a flow boiling in the parallel/tandem microchannel heat sinks, *Energy Convers. Manage.* 148 (2017) 1082–1095.
- [16] A. Radwan, S. Ookawara, S. Mori, M. Ahmed, Uniform cooling for concentrator photovoltaic cells and electronic chips by forced convective boiling in 3D-printed monolithic double-layer microchannel heat sink, *Energy Convers. Manage.* 166 (2018) 356–371.
- [17] I.L. Collins, J.A. Weibel, L. Pan, S.V. Garimella, A permeable-membrane microchannel heat sink made by additive manufacturing, *Int. J. Heat Mass Transf.* 131 (2019) 1174–1183.
- [18] H. Tan, L.W. Wu, M.Y. Wang, Z.H. Yang, P.G. Du, Heat transfer improvement in microchannel heat sink by topology design and optimization for high heat flux chip cooling, *Int. J. Heat Mass Transf.* 129 (2019) 681–689.
- [19] Y.L. Zhai, Z.H. Li, H. Wang, J.X. Xu, Thermodynamic analysis of the effect of channel geometry on heat transfer in double-layered microchannel heat sinks, *Energy Convers. Manage.* 143 (2017) 431–439.
- [20] Y.B. Wang, Z. Kai, C. Zhuo, W. Jie, Effects of the location of the inlet and outlet on heat transfer performance in pin fin CPU heat sink, *Appl. Therm. Eng.* 151 (2019) 506–513.
- [21] A. Katz, S.R. Aakre, M.H. Anderson, D. Ranjan, Experimental investigation of pressure drop and heat transfer in high temperature supercritical CO₂ and helium in a printed-circuit heat exchanger, *Int. J. Heat Mass Transf.* 171 (2021) 121089.
- [22] M.M. Sarafraz, V. Nikkhah, M. Nakhjavani, A. Arya, Thermal performance of a heat sink microchannel working with biologically produced silver-water nanofluid: experimental assessment, *Exp. Therm. Fluid Sci.* 91 (2018) 509–519.
- [23] A.A.A. Arani, O.A. Akbari, M.R. Safaei, A. Marzban, A A A A Airashed, G.R. Ahmadi, T.K. Nguyen, Heat transfer improvement of water/single-wall carbon nanotubes (SWCNT) nanofluid in a novel design of a truncated double-layered microchannel heat sink, *Int. J. Heat Mass Transf.* 113 (2017) 780–795.
- [24] H.M. Ali, W. Arshad, Effect of channel angle of pin-fin heat sink on heat transfer performance using water based graphene nanoplatelets nanofluids, *Int. J. Heat Mass Transf.* 106 (2017) 465–472.
- [25] B. Naranjani, E. Roohi, A. Ebrahimi, Thermal and hydraulic performance analysis of a heat sink with corrugated channels and nanofluids, *J. Therm. Anal. Calorim.* 146 (6) (2021) 2549–2560.
- [26] S.K. Oudah, R.X. Fang, A. Tikadar, A.S. Salman, J.A. Khan, An experimental investigation of the effect of multiple inlet restrictors on the heat transfer and pressure drop in a flow boiling microchannel heat sink, *Int. J. Heat Mass Transf.* 153 (2020) 119582.
- [27] J. Mathew, P.S. Lee, T.Q. Wu, C.R. Yap, Experimental study of flow boiling in a hybrid microchannel-micropin heat sink, *Int. J. Heat Mass Transf.* 135 (2019) 1167–1191.
- [28] M.M. Sarafraz, M. Arjomandi, Thermal performance analysis of a microchannel heat sink cooling with copper oxide-indium (CuO/In) nano-suspensions at high-temperatures, *Appl. Therm. Eng.* 137 (2018) 700–709.
- [29] H. Babar, H.M. Ali, Airfoil shaped pin-fin heat sink: potential evaluation of ferric oxide and titania nanofluids, *Energy Convers. Manage.* 202 (2019) 112194.
- [30] D.X. Deng, L. Chen, W. Wan, T. Fu, X. Huang, Flow boiling performance in pin fin-interconnected reentrant microchannels heat sink in different operational conditions, *Appl. Therm. Eng.* 150 (2019) 1260–1272.
- [31] E.M. Abo-Zahhad, S. Ookawara, A. Radwan, S. Memon, Y. Yang, M.F. El-Kady, A.H. El-Shazly, Flow boiling in a four-compartment heat sink for high-heat flux cooling: a parametric study, *Energy Convers. Manage.* 230 (2021) 113778.
- [32] C. Xu, S.L. Xu, R.D. Eticha, Experimental investigation of thermal performance for pulsating flow in a microchannel heat sink filled with PCM (paraffin/CNT composite), *Energy Convers. Manage.* 236 (2021) 114071.
- [33] C.P. Pan, D.H. Wang, Modeling and experimental verification of the flow characteristics of an active controlled microfluidic valve with annular boundary, *J. Intell. Mater. Syst. Struct.* 27 (16) (2016) 2237–2248.
- [34] L.S. Pan, T.Y. Ng, G.R. Liu, K.Y. Lam, T.Y. Jiang, Analytical solutions for the dynamic analysis of a valveless micropump-a fluid-membrane coupling study, *Sens. Actuators* 93 (2) (2001) 173–181.
- [35] C.J. Morris, F.K. Forster, Optimization of a circular piezoelectric bimorph for a micropump driver, *J. Micromech. Microeng.* 10 (3) (2000) 459–465.
- [36] D.H. Wang, Y.H. Peng, L.K. Tang, H.Q. Yu, A multi-chamber piezoelectric pump based on pumping unit with double circular piezoelectric unimorph actuators, *Smart Mater. Struct.* 30 (9) (2021) 095023.
- [37] E.N. Sieder, G.E. Tate, Heat transfer and pressure drop of liquids in tubes, *Ind. Eng. Chem.* 28 (1936) 1429–1435.